ACS OMEGA

Open Access

http://pubs.acs.org/journal/acsodf

Article

Mechanical Properties and Strength Criteria of Hydrate-Bearing Sediments Considering Clay Minerals

Gege Tang, Rui Jia,* Huilan He, Yiming Li, and Xiaolin Li

Cite This: *ACS Omega* 2024, 9, 46192−46203

Read Online

ACCESS | Metrics & More | Article Recommendations

ABSTRACT: Understanding the effect of clay on the mechanical properties and strength criteria of hydrate-bearing sediments (HBS) is essential for evaluating the safety of clay-rich reservoirs. In this study, a series of triaxial shear tests were conducted to investigate the impacts of clay type and content on the mechanical behavior of I-HBS (hydrate-bearing sediments containing illite) and M-HBS (hydrate-bearing sediments containing montmorillonite). The findings reveal that M-HBS exhibit greater susceptibility to strain hardening compared to I-HBS, accompanied by more extensive volume deformation, and both strain hardening and shear shrinkage intensify with increasing clay content. Moreover, the results demonstrate higher failure strength and Young's modulus in I-HBS than M-HBS. The failure strength of sediments is affected by both the clay content and effective confining pressure, with an established relationship between the failure strength and these two factors. Additionally, the cohesion and internal friction angle of sediments exhibit distinct linear correlations with clay content due to variations in the clay type. The Mohr−Coulomb strength criterion incorporating the clay content is established, enabling the prediction of shear strength in clay-rich hydrate reservoirs. The clay type and content are the cause for different strengths and shear mechanisms of sediments. This research holds significant implications for the safe mining of natural gas clay-rich hydrate reservoirs.

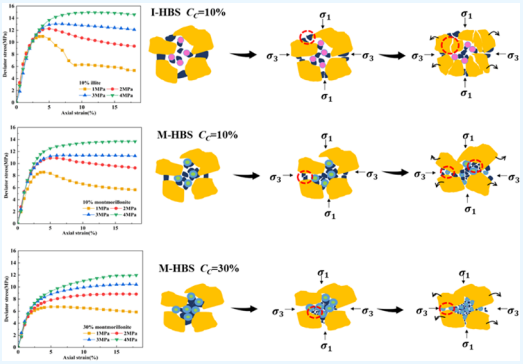

1. INTRODUCTION

As a potential alternative energy source, methane hydrate has the characteristics of high energy density, nonpollution, and wide distribution,[1−5] and several trial productions have been conducted due to its potential.[6−9] However, during the exploitation of marine hydrates, the decomposition of hydrates can weaken the reservoir cementation and lead to strength attenuation, thereby jeopardizing the reservoir stability. This can result in natural disasters such as submarine landslides, large-scale methane gas leakage, and engineering mishaps like deformation of the drilling casing and collapse of the drilling platform.[10−13] Therefore, it is imperative to thoroughly study and evaluate the mechanical stability of gas hydrate reservoirs to facilitate safe, long-term, and large-scale exploitation of gas hydrates.

Natural gas hydrates exist in different types of sediment reservoirs. Previous studies have highlighted that the composition of the host sediment and its particle size distribution significantly influence the mechanical properties of hydrate sediments. The study of methane hydrate sediments with varying particle sizes found that coarser sands exhibit greater lateral deformation and Poisson's ratio compared to fine sands.[14] A hydrate mechanical experiment conducted with or without silt addition and the particle size of silt as experimental variables indicated that the presence of silt, along with larger particle sizes, resulted in an increased vertical load required for hydrate failure.[15] Triaxial shear tests on hydrate sediments composed of two different minerals concluded that sandy hydrate-bearing sediments demonstrate greater failure strength compared to those containing clay.[16] However, under actual reservoir conditions, single sandy or clayey deposits rarely occur, and the results gained from the aforementioned studies cannot be directly applied to a clayey-silty sand reservoir.

The clayey-silty sand hydrate reservoir in the South China Sea with the largest reserves is widely acknowledged as the most challenging to exploit.[17,18] The exploration area is predominantly composed of fine particles and clay minerals; the main clay types are montmorillonite and illite, with the clay content showing variations across different locations.[19−23] The diversity and concentration of clay minerals modify the material composition and particle size distribution of the surrounding sediments, thereby influencing the mechanical characteristics. Based on this, the mechanical behavior of hydrate-bearing sediments taking into account content variations in illite and

Received: July 22, 2024
Revised: October 23, 2024
Accepted: October 24, 2024
Published: November 4, 2024

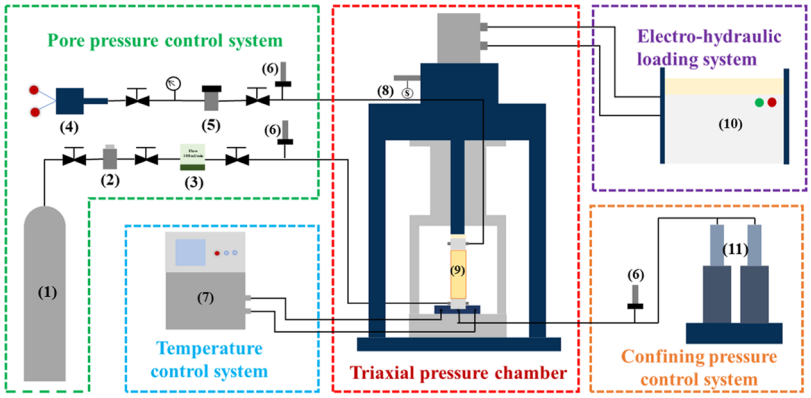

Figure 1. Schematic diagram of the SHW-3 triaxial shear test device.

montmorillonite under different effective confining pressures was studied, which indicated that both the clay type and clay content play significant roles in determining the failure strength and deformation characteristics of clayey-silty sediments.[24] The type and content of clay minerals significantly influence the synthesis of hydrates within sediment pores, resulting in the difference in hydrate saturation.[25,26] In addition, hydrate saturation is a crucial factor influencing the mechanical properties of hydrate deposits, which cannot be overlooked.[27−29] Consequently, it is imperative to study the influence of both the type and content of clay minerals at consistent hydrate saturation to understand the mechanical behavior of clay-silt hydrate reservoirs.

Additionally, research into the constitutive models of hydrate sediments has also been conducted. Taking into account factors such as hydrate saturation,[30] temperature,[31] and confining pressure,[32] some researchers have developed a nonlinear elastic constitutive model for hydrate-bearing sandy sediments based on the Dundun-Chang model. Other researchers have established an elastic−plastic constitutive model for hydrate-bearing sediments, drawing on the Cam-Clay model and taking into account variables such as temperature,[33] pressure[34] and the state of hydrate occurrence.[35] The linear expression of the Mohr−Coulomb intensity facilitates the derivation of analytical solutions. Numerous experimental findings demonstrate that the Mohr−Coulomb strength criterion is highly applicable and effective in the field of soil mechanics. Mohr−Coulomb strength criteria applicable to quartz sand reservoir[36] and Toyoura sand reservoir[37] were established, respectively. In addition, the strength criteria of clay-containing hydrate sediments considering effective confining pressure[38] and hydrate saturation[39] were developed. Although domestic and foreign scholars have proposed a constitutive model suitable for hydrate reservoirs, most of the modified parameters are pressure, temperature, hydrate saturation, and other conditions. However, the significant factor of clay minerals has yet to be incorporated into these models.

In this paper, the impact of various clay mineral types and contents on the mechanical properties of the artificially prepared clayey-silt hydrate-bearing sediments under the same hydrate saturation conditions were studied. Specifically, impact mechanisms of illite and montmorillonite on the strength and deformation properties of these sediments were analyzed, and the mathematical relationship between the failure strength, clay content, and effective confining pressure was obtained. The clay content was also introduced into the Mohr−Coulomb strength criterion to develop a constitutive model which could describe the mechanical behavior of clayey-silt reservoirs. In addition, the results also revealed the strength and shear mechanism of sediments containing different clay mineral hydrate-bearing sediments.

2. EXPERIMENTAL SECTION

2.1. Experimental Apparatus. This study used a self-developed triaxial apparatus with a low-temperature and high-pressure environment, which can form and decompose natural gas hydrates in situ (Figure 1). The apparatus consists of six systems: electro-hydraulic loading system, triaxial pressure chamber, pore pressure control system, confining pressure control system, temperature control system, and data acquisition system. The maximum confining pressure is 50 MPa, and the accuracy is 0.01 MPa. The axial load is controlled by the electro-hydraulic loading system, which can provide a maximum axial load of 200 KN. The thermostatic water bath is used to control the temperature and ranges from −30 to 100 °C, with an accuracy of 0.5 °C. All of the data during the tests are recorded by a data acquisition system.

2.2. Sample Preparation. According to the reservoir characteristics of the Shenhu Sea area in the South China Sea, the target porosity was set at 0.4 and hydrate saturation at 30%, selecting illite and montmorillonite as target clay minerals in this study. Then, different contents of illite and montmorillonite were mixed with quartz sand and distilled water to remodel I-HBS and M-HBS, respectively. The mixture was equally filled into the mold in 5 times by the compaction method, and a cylindrical specimen with a diameter of 50 mm and a height of 100 mm was obtained by an electro-hydraulic stripper. Then, the sample, which was sealed with a rubber film and a sealing ring, was installed in the triaxial chamber. After the sample was prepared, the pressure chamber was filled with silicone oil and provided with 2 MPa confining pressure. Then, methane gas was injected at a constant rate until the pore pressure reached 6 MPa, at which time the effective confining pressure was reduced to 0.5 MPa. Finally, the temperature in the triaxial cell was set to 274.15 K. In this study, the excess gas method was used to synthesize hydrates, and when the data monitored by the gas

https://doi.org/10.1021/acsomega.4c06735
ACS Omega 2024, 9, 46192−46203

Table 1. Triaxial Shear Test Conditions for Sediments with Different Clay Contents

runs	clay type	m_s/m_c	T (K)	S_h (%)	P_P (MPa)	P_C (MPa)	P'_c (MPa)	ε_a (%/min)
1	illite	9:1	274.15	30.01	6	7	1	1
2				29.84		8	2	
3				29.99		9	3	
4				29.79		10	4	
5		8:2	274.15	31.3	6	7	1	1
6				29.71		8	2	
7				29.81		9	3	
8				30.26		10	4	
9		7:3	274.15	30.6	6	7	1	1
10				31.5		8	2	
11				30.68		9	3	
12				30.52		10	4	
13	montmorillonite	9:1	274.15	28.9	6	7	1	1
14				30.18		8	2	
15				28.5		9	3	
16				30.58		10	4	
17		8:2	274.15	29.1	6	7	1	1
18				30.36		8	2	
19				29.33		9	3	
20				30.34		10	4	
21		7:3	274.15	30.2	6	7	1	1
22				31.06		8	2	
23				29.68		9	3	
24				31.02		10	4	

m_s: quality of quartz sand; m_c: quality of clay; S_h: hydrate saturation; P_P: pore pressure; P_C: confining pressure; $P'_c(P'_c = P_C - P_P)$: effective confining pressure; ε_a: strain rate.

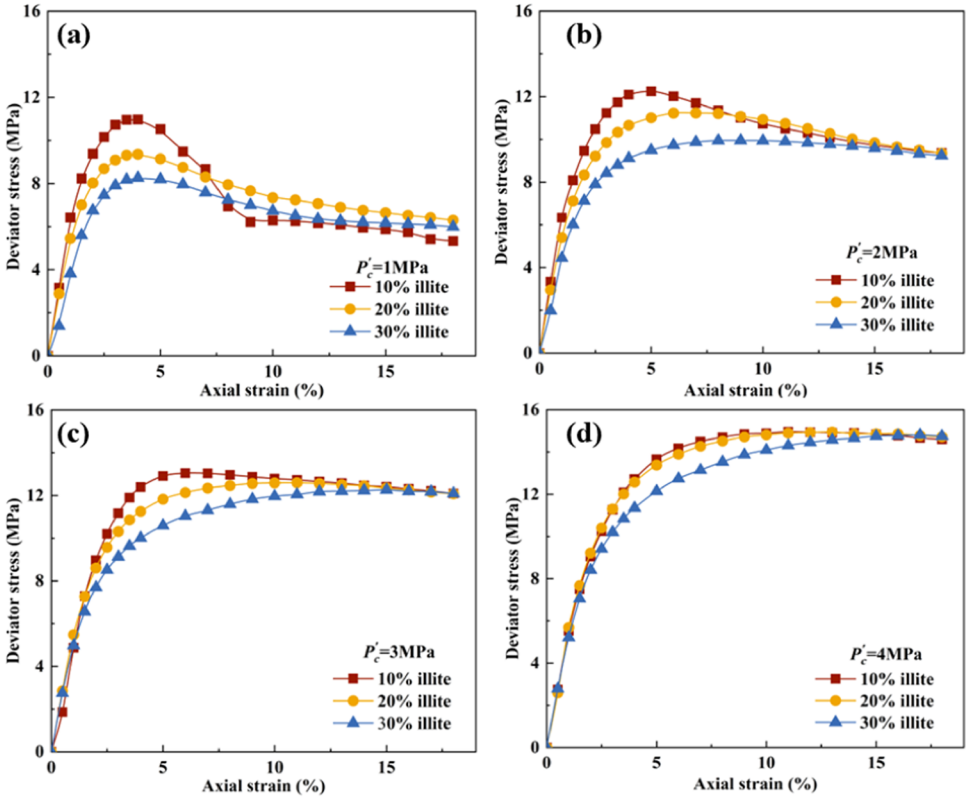

Figure 2. Stress−strain curves of I-HBS under different effective confining pressures: (a) 1 MPa; (b) 2 MPa; (c) 3 MPa; (d) 4 MPa.

flow meter was 0, it was determined that the hydrate synthesis was complete. After the sediment was consolidated for 12 h, 24 runs of triaxial shear tests were carried out on sediments with different clay contents. The detailed test conditions are shown in Table 1.

https://doi.org/10.1021/acsomega.4c06735
ACS Omega 2024, 9, 46192−46203

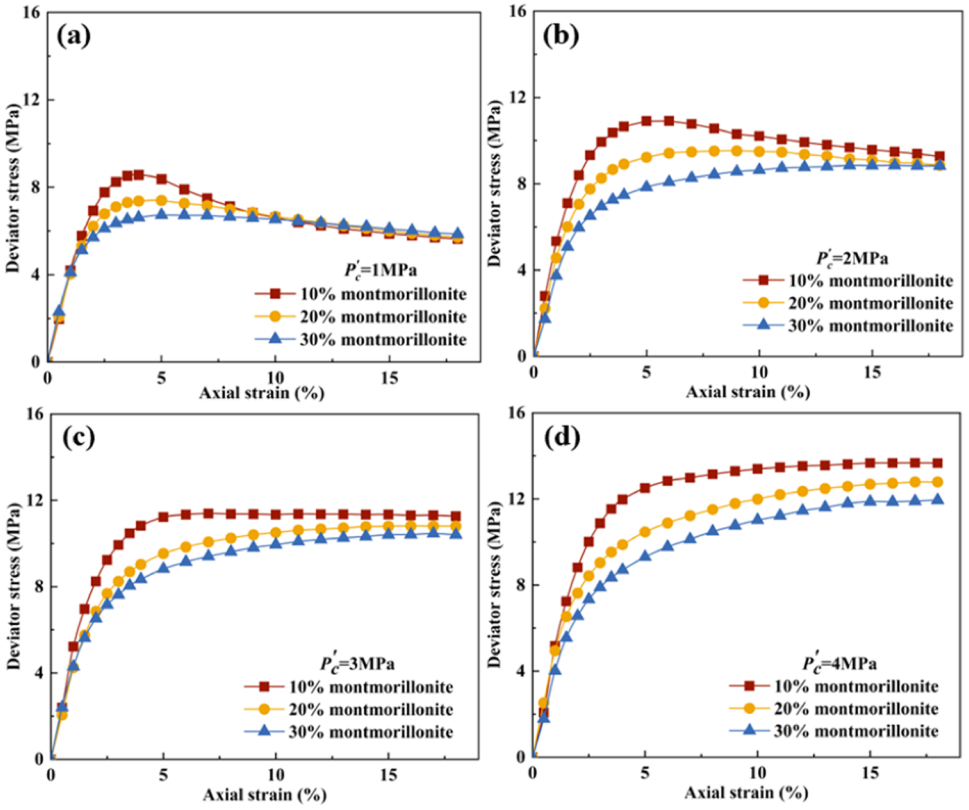

Figure 3. Stress−strain curves of M-HBS under different effective confining pressures: (a) 1 MPa; (b) 2 MPa; (c) 3 MPa; (d) 4 MPa.

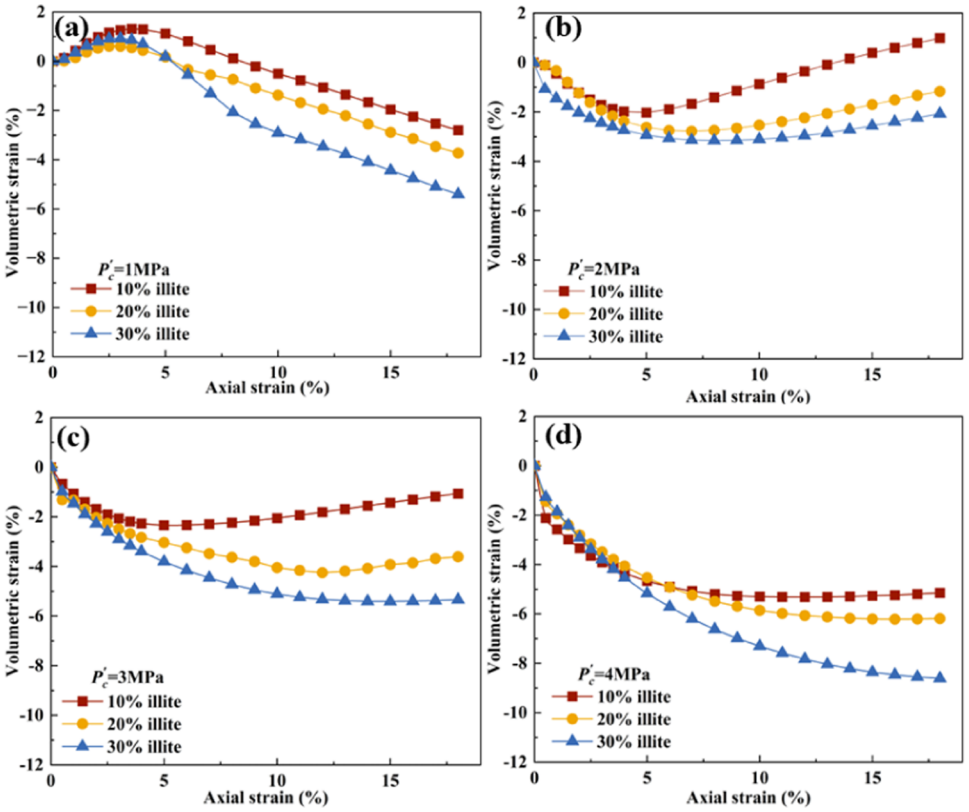

Figure 4. Volume−strain curves of I-HBS under different effective confining pressures: (a) 1 MPa; (b) 2 MPa; (c) 3 MPa; (d) 4 MPa.

https://doi.org/10.1021/acsomega.4c06735
ACS Omega 2024, 9, 46192−46203

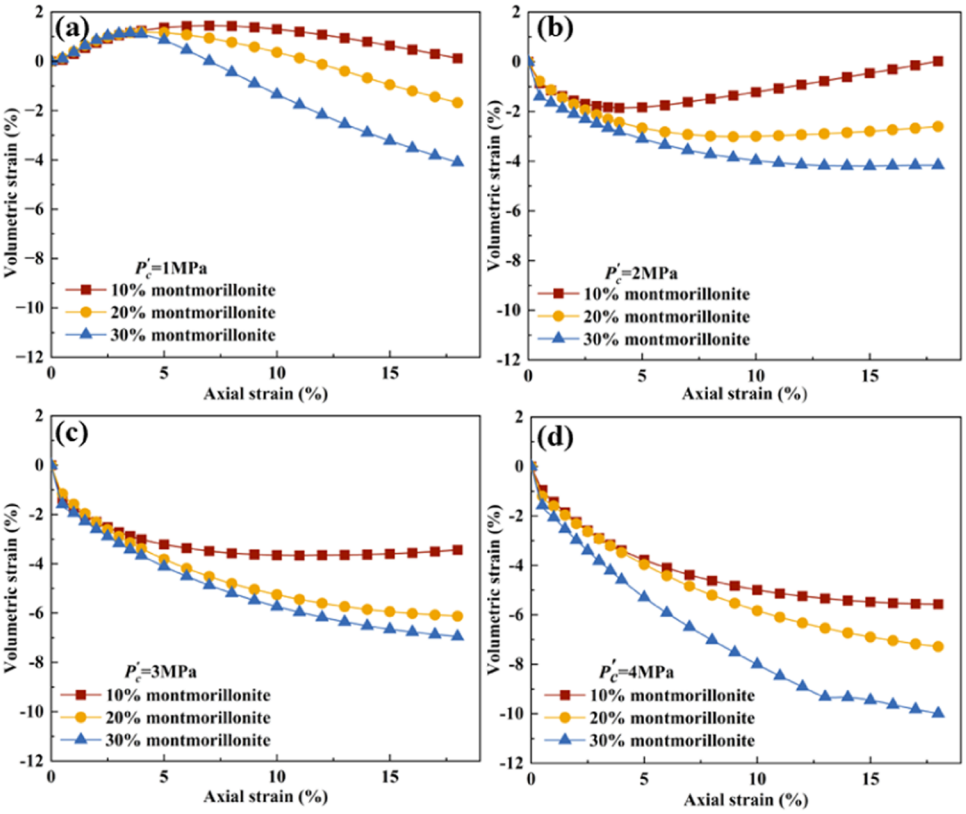

Figure 5. Volume−strain curves of M-HBS under different effective confining pressures: (a) 1 MPa; (b) 2 MPa; (c) 3 MPa; (d) 4 MPa.

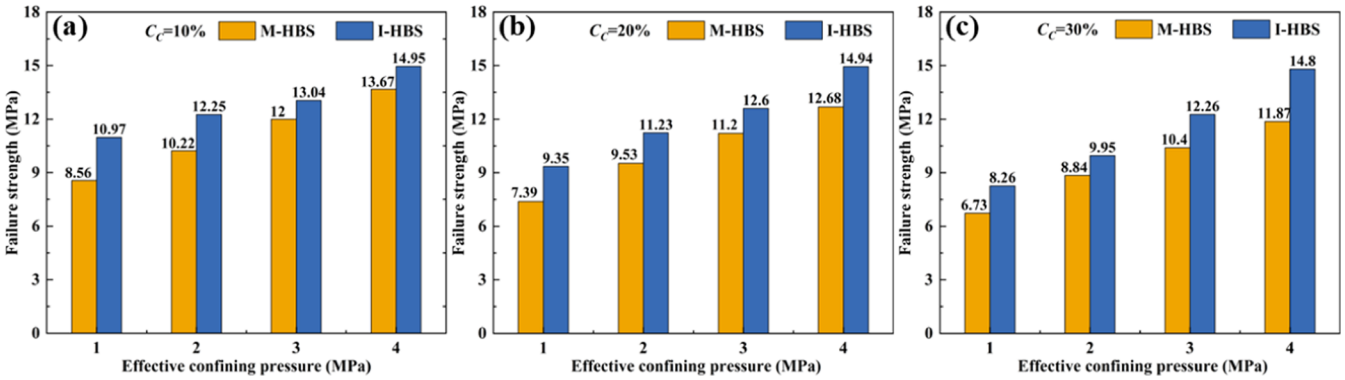

Figure 6. Failure strength at different clay contents: (a) C_C = 10%; (b) C_C = 20%; (c) C_C = 30% (C_C: clay content).

3. RESULTS AND DISCUSSION

3.1. Stress and Strain Characteristics and Volume−Strain Response. Figures 2 and 3 show the stress−strain relationships of I-HBS and M-HBS, respectively, under different effective confining pressures of 1, 2, 3, and 4 MPa. It can be seen that all stress−strain curves exhibit nonlinear relationships. At the beginning of loading, the deviator stress increases rapidly with the increase of axial strain, and then two phenomena occur: the deviator stress decreases after reaching the peak value (strain softening) or the deviator stress continues to increase at a small rate (strain hardening). As the effective confining pressure increases, the stress−strain behavior of I-HBS exhibits strain softening, whereas M-HBS transition from strain softening to strain hardening. At lower confining pressures, the strain softening effect in I-HBS is more pronounced, while at higher confining pressures, the strain hardening in M-HBS becomes significantly more evident. This distinction can be attributed to the larger specific surface area of montmorillonite compared to illite, which facilitates a greater number of contact points between hydrate and sediment particles,[40] thereby reducing the potential for displacement. Additionally, an increase in clay content tends to suppress strain softening while amplifying strain hardening, a phenomenon likely due to the enhanced interparticle contact fostered by the presence of more fine clay particles.

Figures 4 and 5 show the volume−strain relationship of I-HBS and M-HBS, respectively, at effective confining pressures of 1, 2, 3, and 4 MPa. Under low confining pressures, both I-HBS and M-HBS initially exhibit shrinkage, followed by dilatancy, whereas under high confining pressures, they both demonstrate shear contraction. This behavior is attributed to the elevated confining pressures that restrict the particle rotation and enhance the bonding between soil and hydrate particles.[41] After loading completely, the volume of I-HBS exceeds that of

https://doi.org/10.1021/acsomega.4c06735
ACS Omega 2024, 9, 46192−46203

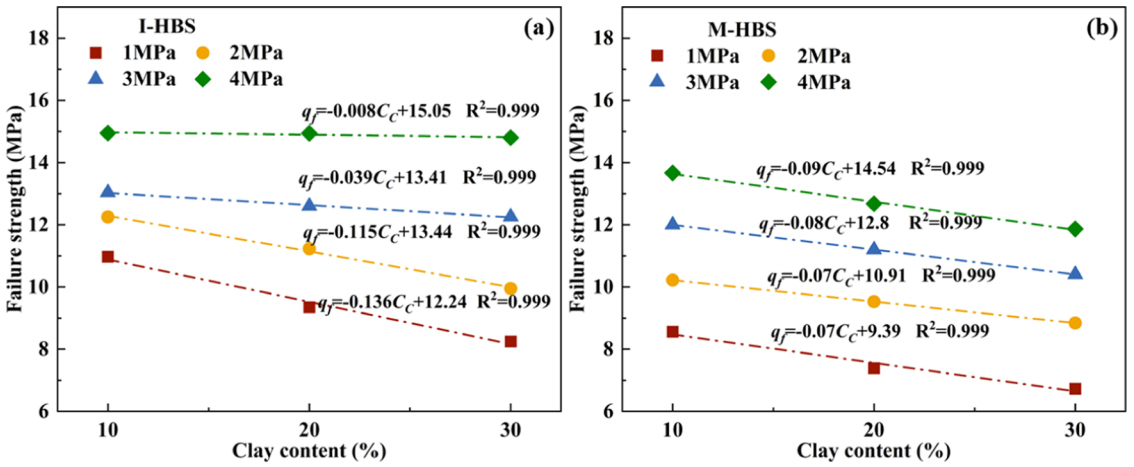

Figure 7. Failure strength fitting under different effective confining pressures: (a) I-HBS; (b) M-HBS.

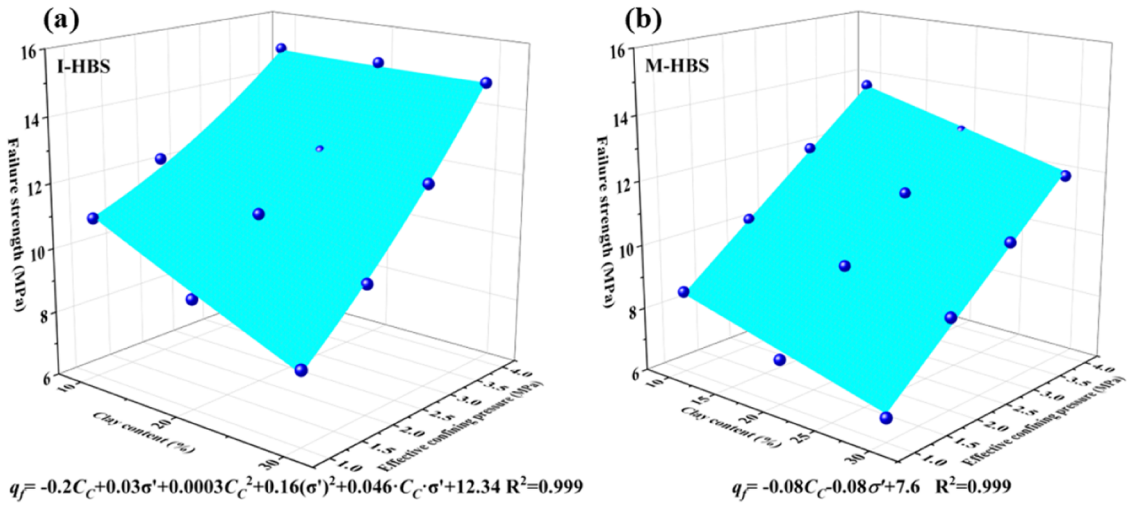

Figure 8. Plane fitting of failure strength with clay content and effective confining pressure: (a) I-HBS; (b) M-HBS.

M-HBS, which is explained by the latter's greater pore space allowing for more effective particle rearrangement and less radial tumbling. The increase of the clay content will inhibit the dilatancy behavior and aggravate the shear shrinkage behavior. Under low confining pressures, the axial strain corresponding to the dilatancy behavior increases with an increase of the clay content. After shear, the sample volume inversely correlates with the clay content, as during compression fine clay particles more readily move through adjacent particles into pore spaces for rearrangement.

3.2. Failure Strength and Young's Modulus. *3.2.1. Failure Strength.* The strengths of I-HBS and M-HBS with different clay contents are shown in Figure 6. For strain-softening specimens, the maximum deviator stress corresponding to the peak value of the stress−strain curve is taken as the failure strength. For strain-hardening specimens, 15% axial strain is taken as the failure state of the specimen, and the deviator stress corresponding to 15% axial strain in the stress−strain curve is taken as the failure strength. The failure strength of I-HBS is higher than that of M-HBS under the identical effective confining pressure. This phenomenon can be attributed to illite having relatively weak hydrophilicity, the presence of a slim bound water film, and a reduced number of interfacing points between clay particles and quartz sand. Concurrently, hydrates form partially on the surface of illite and partially on the surface of quartz sand. In such instances, the cementation of hydrate takes precedence, overshadowing the diminution in frictional strength brought about by the clay particles' lubricative action. Conversely, montmorillonite shows pronounced hydrophilicity, leading to the formation of a substantially bound water film. This results in extensive contact between quartz sand particles and clay particles, with the majority of hydrates forming on montmorillonite's surface. At this point, the lubricative effect of the clay may emerge as the predominant factor. The failure strength is affected by both the type of clay and the effective confining pressure. This indicates that enhancing the effective confining pressure amplifies the impact of the type of clay on the sediment failure strength.

The failure strength fitting curves of I-HBS and M-HBS under different confining pressures were drawn as shown in Figure 7. The slopes of the fitting formulas were uniformly negative, representing the weakening effect of the clay content on the failure strength. The failure strength of both I-HBS and M-HBS decreases with an increase of clay content. This is attributed to the enhanced interparticle contact and the pronounced lubrication effect that accompanies a higher clay content.[42] For I-HBS, with the increase of the effective confining pressure, the weakening effect of clay content on the failure strength decreases. The influence of effective confining pressure on the material's resistance to damage becomes increasingly significant

https://doi.org/10.1021/acsomega.4c06735
ACS Omega 2024, 9, 46192−46203

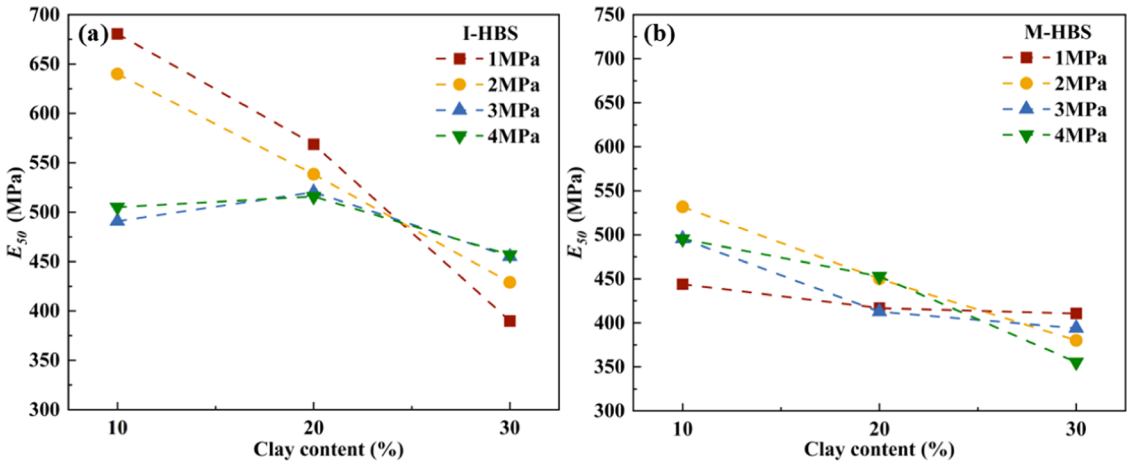

Figure 9. Young's modulus under different effective confining pressures: (a) I-HBS; (b) M-HBS.

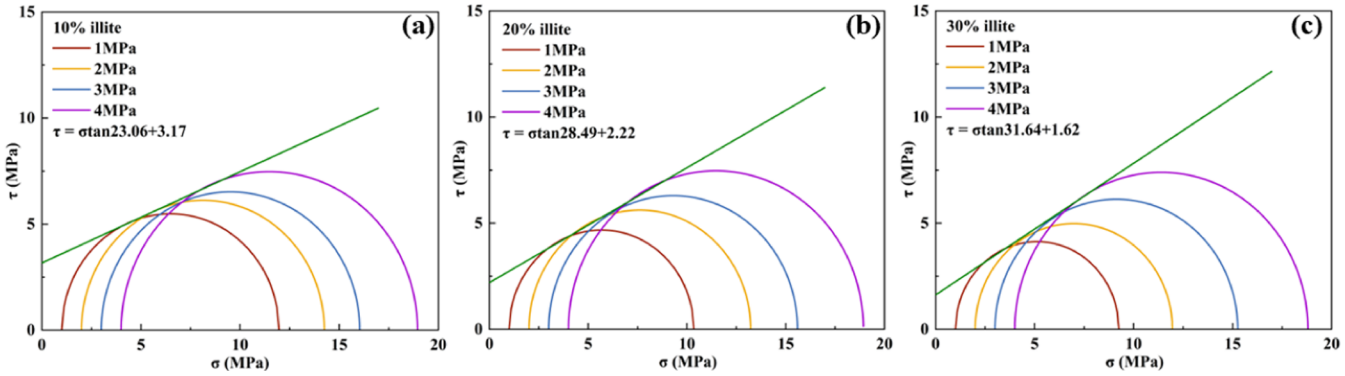

Figure 10. Stress Mohr circle of host sediments with different illite contents: (a) 10% illite; (b) 20% illite; (c) 30% illite.

with a higher clay content. Conversely, for M-HBS, the decline in failure strength due to a higher clay content remains consistent, irrespective of the effective confining pressure. This pattern suggests that the response of failure strength to variations in the illite content is particularly sensitive to changes in the effective confining pressure.

In addition, the plane fitting of the failure strength under the combined influence of the clay content and effective confining pressure was carried out in this paper, as shown in Figure 8. The fitting accuracy for both I-HBS and M-HBS achieved 0.999, indicating excellent agreement with the observed data. Consequently, a fitting formula for predicting failure strength under the combined influence of clay content and effective confining pressure was derived, as detailed in eq 1

$$(q_f)_{\text{sediment}} = \lambda C_C + \mu\sigma' + \xi C_C^2 + \nu(\sigma')^2 + \omega \cdot C_C \cdot \sigma' + \kappa \quad (1)$$

where q_f is the failure strength; C_C is the clay content; σ' is the effective confining pressure; λ, μ, ξ, ν, ω, and κ are related parameters. When the sediment is I-HBS, $\lambda = -0.2$, $\mu = 0.03$, $\xi = 0.0003$, $\nu = 0.16$, $\omega = 0.046$, and $\kappa = 12.34$, and when the sediment is M-HBS, $\lambda = -0.08$, $\mu = -0.08$, $\xi = 0$, $\nu = 0$, $\omega = 0$, and $\kappa = 7.6$.

The above fitting formula can be used to estimate the shear strength of clayey-silt reservoirs with different clay contents when the effective confining pressure is known.

3.2.2. Young's Modulus. Young's modulus is a physical quantity that describes the relationship between stress and strain in the elastic range. Due to the nonlinear stress−strain relationship of the reconstructed hydrate-bearing clayey-silt sediment, the elastic stage is not obvious. Consequently, Young's modulus (E_{50}) was used as the stiffness of hydrate-bearing sediments, that is, the ratio of 50% of the sample's failure strength to the corresponding axial strain. Figure 9 illustrates the stiffness curves of various hydrate-bearing sediments with the clay content. It is evident that both the clay content and effective confining pressure significantly influence the stiffness of the sediment. Notably, the Young's modulus for I-HBS generally surpasses that of M-HBS. This discrepancy can be attributed to the montmorillonite's thicker bound water film on its surface, which enhances the lubrication effect among sediment particles, thereby weakening the sample's resistance to deformation. For I-HBS, stiffness declines as the clay content increases under low effective confining pressures. However, at high effective confining pressures, stiffness initially rises before decreasing with an increase in the clay content. This phenomenon occurs because, at low clay contents, the impact of high effective confining pressure on particle mobility exceeds the lubricative effect of clay on adjacent particles. Conversely, at high clay contents, lubrication between particles becomes the dominating factor. For M-HBS, the stiffness and clay content exhibit a consistently negative correlation. This is due to montmorillonite's enhanced hydrophilicity, which leads to the formation of a thicker water film on the particle surfaces and an increase in contact points between the clay particles and quartz sand.[43] Consequently, the lubrication effect of clay on the particles predominates regardless of the clay content.

https://doi.org/10.1021/acsomega.4c06735
ACS Omega 2024, 9, 46192−46203

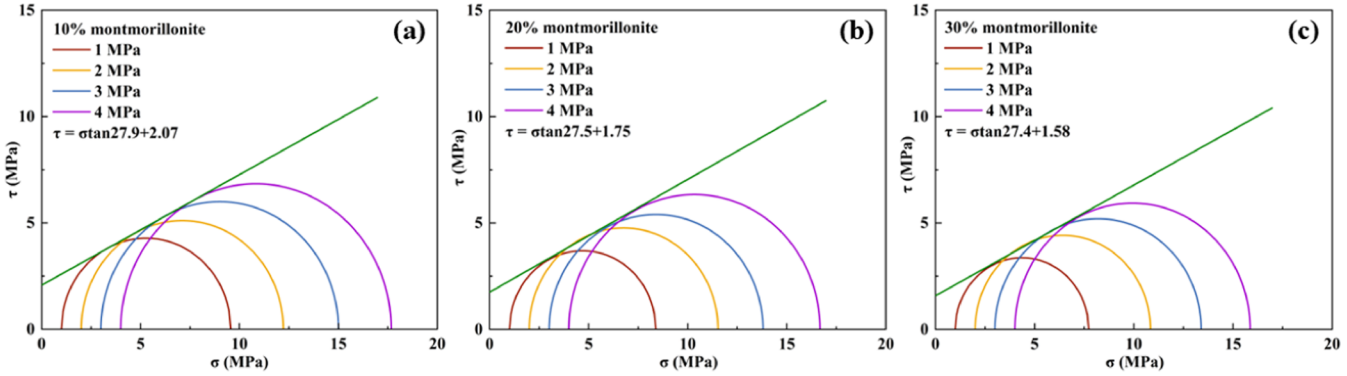

Figure 11. Stress Mohr circle of host sediments with different montmorillonite contents: (a) 10% montmorillonite; (b) 20% montmorillonite; (c) 30% montmorillonite.

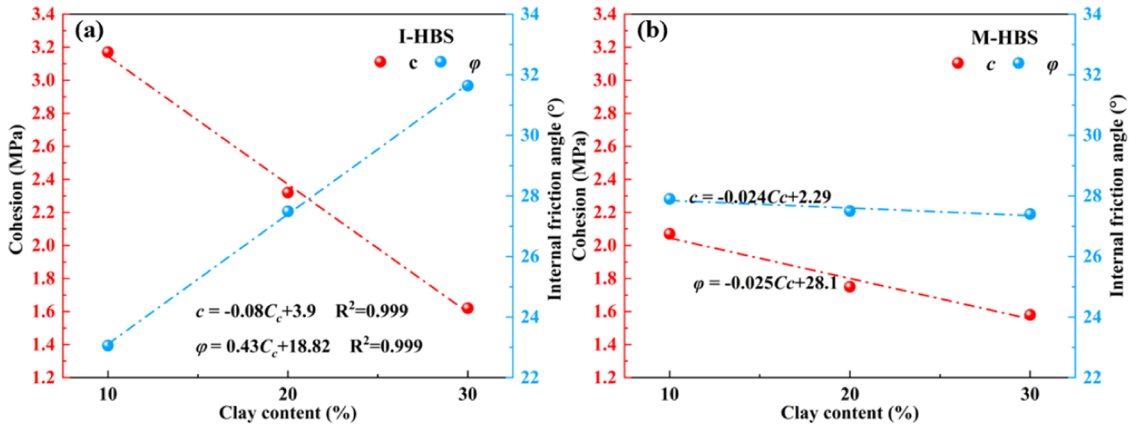

Figure 12. Relationship between the cohesion, internal friction angle, and clay content: (a) I-HBS; (b) M-HBS.

3.3. Cohesion and Internal Friction Angle. Mohr envelopes of I-HBS and M-HBS obtained by Mohr−Coulomb criteria are shown in Figures 10 and 11, respectively. It can be observed that the higher the clay content, the smaller the radius of the Moire circle, and the smaller the damage strength. The intercept and slope of the envelope are the cohesion and the tangent of the internal friction angle of the sample, respectively.

Figure 12 shows that the cohesion and internal friction angle of hydrate-bearing clayey-silt sediments are affected by both the clay mineral type and clay content. The cohesion and internal friction angle of I-HBS exhibit a heightened sensitivity to the change of the clay content. For both I-HBS and M-HBS, there is a linear negative correlation between the cohesion and the clay content. This trend is attributed to the increase in the clay content, which, owing to the water absorption properties of clay minerals, results in a predominant formation of hydrates on the surface of clay particles as opposed to the surface of quartz sand. Consequently, this distribution leads to a decrease in the overall connectivity within the sample. The internal friction angle displayed divergent trends, being positively correlated with the content of illite and negatively with that of montmorillonite. This divergence arises because the water-absorbing expansion of illite compresses the distance between particles and thus changes the contact state between particles,[44] which increases the internal friction angle. On the other hand, montmorillonite's more pronounced water absorption and expansion capabilities, combined with its larger specific surface area compared to illite, result in the formation of a thicker bonded water film in hydrate-bearing sediments containing montmorillonite. The thicker film intensifies the lubricative effect of the clay, leading to a reduction in the internal friction angle.

3.4. Strength Criterion. *3.4.1. Establishment of The Strength Criterion.* Mohr−Coulomb theory, also known as Coulomb strength theory, can reflect the strength characteristics of rocks and soil. The specific formula is as follows

$$\sigma_1 - \sigma_3 = \frac{2}{1 - \sin\varphi}(c\cdot\cos\varphi + \sigma_3 \sin\varphi) \tag{2}$$

Taking clay content as the main variable, the relationships between the sediment strength parameter φ and the clay content (eq 3) and between c and the clay content (eq 4) were obtained, which were incorporated into the Mohr−Coulomb failure criterion (eq 2), and the Mohr−Coulomb strength criterion applicable to shaly silt hydrate deposits was obtained. The revised Mohr−Coulomb criterion is shown in eq 5

$$\varphi(C_C) = \alpha C_C + \beta \tag{3}$$

$$c(C_C) = aC_C + b \tag{4}$$

$$(\sigma_1 - \sigma_3)_{\text{sediment}} = 2\frac{[(aC_C + b)\cos(\alpha C_C + \beta) + \sigma_3 \sin(\alpha C_C + \beta)]}{1 - \sin(\alpha C_C + \beta)} \tag{5}$$

where C_C is the clay content; φ is the internal friction angle, c is cohesion; α, β, a, and b are related parameters. When the sediment is I-HBS, $\alpha = 0.43$, $\beta = 18.82$, $a = -0.08$, and $b = 3.9$;

https://doi.org/10.1021/acsomega.4c06735
ACS Omega 2024, 9, 46192−46203

Table 2. Triaxial Shear Test Conditions for I-HBS and M-HBS Samples Having a Clay Content of 25%

test	clay type	m_s/m_c	T (K)	S_h (%)	P_P (MPa)	P_C (MPa)	P'_c (MPa)	ε_a (%/min)
1	illite	3:1	274.15	30.12	6	7	1	1
2				30.99		8	2	
3				30.85		9	3	
4				30.11		10	4	
5	montmorillonite	3:1	274.15	29.89	6	7	1	1
6				30.68		8	2	
7				29.25		9	3	
8				30.6		10	4	

when the sediment is M-HBS, $\alpha = -0.025$, $\beta = 28.1$, $a = -0.024$, and $b = 2.29$.

The modified criterion is different from the traditional Mohr−Coulomb criterion, and the model can be used to predict the shear strength of silty-silt hydrate reservoirs with different clay contents.

3.4.2. Model Validation. Based on the defined strength criteria, the strength of hydrate-bearing clayey-silt sediment can be determined for varying clay contents. To verify the accuracy of the model, triaxial shear experiments were conducted on both I-HBS and M-HBS samples, specifically chosen to have a clay content of 25%, and experimental conditions are shown in Table 2. The experimental value and the predicted strength values of these samples were then compared, as illustrated in Figure 13. The forecast failure strength closely aligns with the empirical data, and the maximum error is 2.8%.

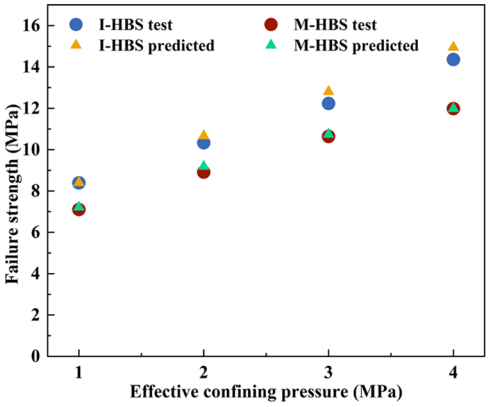

Figure 13. Comparison of test and predicted strengths.

3.5. Mechanism Analysis. Illite and montmorillonite demonstrate distinct water absorption behaviors owing to their unique structural differences.[45] This results in variations in the locations where hydrates form within the sediment, thereby influencing the strength and shear mechanisms of sediments. Figure 14 illustrates a schematic representation of particle movement during the shear processes of I-HBS and M-HBS.

For I-HBS, the relatively low hydrophilicity results in a thinner bound water film, leading to hydrates predominantly forming between quartz sand grains, with a minor portion developing on the surfaces of clay minerals. These hydrates act as a cement between the quartz sand grains, creating a continuous skeletal structure that significantly enhances the sediment's strength. Conversely, for M-HBS, montmorillonite's strong hydrophilicity means hydrates are primarily formed on the clay surface within pores, rather than between quartz sand grains. This difference leads to a reduction in both the binding and skeletal reinforcement provided by the hydrates, thus reducing the strength of M-HBS. Moreover, the presence of a thicker bound water film on montmorillonite surfaces increases its lubricative effect on sediment particles compared with illite, further decreasing the sediment strength.

During the initial stage of I-HBS shear, the hydrate connection between quartz sand particles inhibits the reorientation of these grains, preventing further compression of pore spaces. As stress levels increase, the hydrates binding to the quartz sands are the first to fracture, losing the connection. The fragmented hydrates then enter the pore space, compelling the quartz sand grains to rotate radially or even fracture, which leads to strain softening. In the initial stage of M-HBS shear, the weak cementation between quartz sand particles is destroyed first. As the stress continues to increase, the hydrates nestled among the clay minerals are incrementally compressed and fractured. In addition, because the clay particles are relatively soft, some clay particles will break after being squeezed. These fragmented clay particles then navigate through adjacent particles into a large particle pore space, enhancing the compactness of the specimen and thereby exhibiting strain hardening.

By comparing Figure 14b,c, it becomes evident that as the clay content increases, the pore spaces are increasingly occupied by fine-grained clay, leading to the formation of additional hydrates on the surfaces of clay minerals. At the initial shearing stage, the pore space of quartz sand rich in clay content is the first to undergo compression. With continuous loading, there is not enough pore space for the quartz sand to move, resulting in the clay minerals and surface-generated hydrates being further compacted by the quartz sand grains. In comparison to samples with a lower clay content, those with a higher content of clay exhibit a greater number of hydrate and clay particles undergoing breakage, resulting in sediments that exhibit lower strength.

4. CONCLUSIONS

In this work, the effect of clay mineral types and contents on the mechanical properties of hydrate-bearing sediments were studied under different effective confining pressures, and the following conclusions can be reached:

(1) M-HBS exhibit a greater susceptibility to strain hardening and more significant volume deformation compared to I-HBS. As the clay content increases, an increased number of fine clay particles occupy the pore spaces, aggravating the strain hardening in hydrate-bearing sediments.

(2) The failure strength and Young's modulus of I-HBS surpass those of M-HBS when both are subjected to identical hydrate saturation. Both the clay content and the effective confining pressure influence the failure strength, demonstrating a linear correlation between the clay content and effective confining pressure.

https://doi.org/10.1021/acsomega.4c06735
ACS Omega 2024, 9, 46192−46203

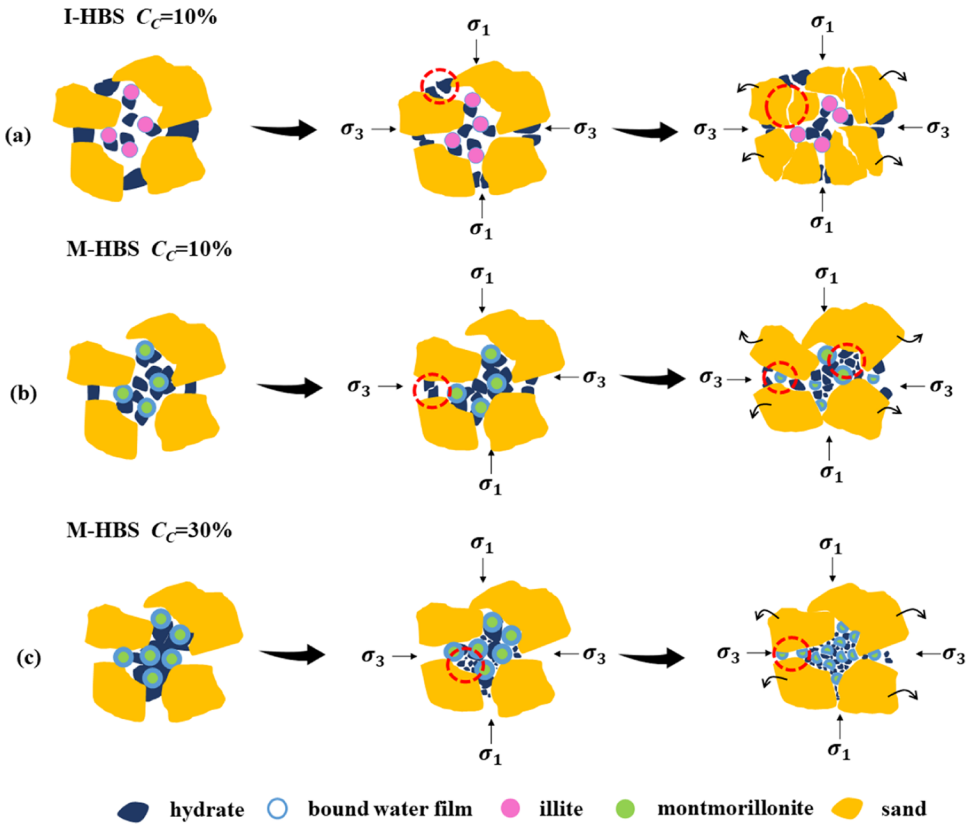

Figure 14. I-HBS and M-HBS shear schematics.

(3) Cohesion and internal friction angle are linearly related to the clay content. The cohesion decreases with the increase of clay content, and the internal friction angle shows a different trend, which positively correlates with the illite content and negatively correlates with the montmorillonite content. The Mohr−Coulomb strength criterion considering the clay content is established.

(4) Illite and montmorillonite produce different thickness bound water films due to different hydrophilicities. Montmorillonite, with its thicker bound water film, enhances the lubrication between M-HBS particles compared to illite. The diversity of clay mineral type and content can alter the sites of hydrate formation, thereby differently impacting the strength of hydrate-bearing sediments.

AUTHOR INFORMATION

Corresponding Author

Rui Jia − *College of Construction Engineering, Jilin University, Changchun 130021, China; Key Lab of Ministry of Natural Resources for Drilling and Exploitation Technology in Complex Conditions, Jilin University, Changchun 130021, China*; Email: jiarui@jlu.edu.cn

Authors

Gege Tang − *College of Construction Engineering, Jilin University, Changchun 130021, China; Key Lab of Ministry of Natural Resources for Drilling and Exploitation Technology in Complex Conditions, Jilin University, Changchun 130021, China*; orcid.org/0009-0007-1607-8549

Huilan He − *Jinshi Drilltech Co., Ltd, Tangshan 063000, China*

Yiming Li − *College of Construction Engineering, Jilin University, Changchun 130021, China; Key Lab of Ministry of Natural Resources for Drilling and Exploitation Technology in Complex Conditions, Jilin University, Changchun 130021, China*

Xiaolin Li − *College of Construction Engineering, Jilin University, Changchun 130021, China*

Complete contact information is available at: https://pubs.acs.org/10.1021/acsomega.4c06735

Author Contributions

G.T.: formal analysis, validation, methodology, data curation, investigation, writing—original draft. R.J.: project administration, supervision, conceptualization, writing—review and editing. H.H.: funding acquisition. Y.L.: investigation, writing—review and editing. X.L.: writing—review and editing.

Notes

The authors declare no competing financial interest.

ACKNOWLEDGMENTS

This work was supported by the National Natural Science Foundation of China (Grant Nos. 51890914 and 42102346) and a Key Lab of Ministry of Natural Resources for Drilling and Exploitation Technology in Complex Conditions and Jinshi Drilltech Co., Ltd. Joint Open Project (Grant No. FZJS230102).

REFERENCES

(1) Englezos, P. Clathrate hydrates. *Ind. Eng. Chem. Res.* **1993**, *32* (7), 1251−1274.

(2) Moridis, G. J.; Collett, T. S.; Boswell, R.; Kurihara, M.; Reagan, M. T.; Koh, C.; Sloan, E. D. Toward production from gas hydrates: current status, assessment of resources, and simulation-based evaluation of

technology and potential. *SPE Reservoir Eval. Eng.* **2009**, *12* (05), 745−771.
(3) Xu, C.-G.; Li, X.-S. Research progress of methane production from natural gas hydrates. *RSC Adv.* **2015**, *5* (67), 54672−54699.
(4) Zhao, J.; Liu, D.; Yang, M.; Song, Y. Analysis of heat transfer effects on gas production from methane hydrate by depressurization. *Int. J. Heat Mass Transfer* **2014**, *77*, 529−541.
(5) Lei, J.; Guo, W.; Yang, X.; Zhang, P.; Jia, R.; Wang, Y. Parameters optimization of storage capacity of hole-bottom freezing sampling technique for natural gas hydrates. *Adv. Geo-Energy Res.* **2024**, *12* (1), 66 DOI: 10.46690/ager.2024.04.06.
(6) Makogon, Y.; Omelchenko, R. Commercial gas production from Messoyakha deposit in hydrate conditions. *J. Nat. Gas Sci. Eng.* **2013**, *11*, 1−6.
(7) Kurihara, M.; Sato, A.; Funatsu, K.; Ouchi, H.; Yamamoto, K.; Numasawa, M.et al., Eds.; *Analysis of Production Data for 2007/2008 Mallik Gas Hydrate Production Tests in Canada*, SPE International Oil and Gas Conference and Exhibition in China; SPE, 2010.
(8) Yamamoto, K. Overview and introduction: Pressure core-sampling and analyses in the 2012−2013 MH21 offshore test of gas production from methane hydrates in the eastern Nankai Trough. *Mar. Pet. Geol.* **2015**, *66*, 296−309.
(9) Li, J.-f.; Ye, J.-l.; Qin, X.-w.; Qiu, H.-j.; Wu, N.-y.; Lu, H.-l.; et al. The first offshore natural gas hydrate production test in South China Sea. *China Geol.* **2018**, *1* (1), 5−16.
(10) Glasby, G. Potential impact on climate of the exploitation of methane hydrate deposits offshore. *Mar. Pet. Geol.* **2003**, *20* (2), 163−175.
(11) Brown, H. E.; Holbrook, W. S.; Hornbach, M. J.; Nealon, J. Slide structure and role of gas hydrate at the northern boundary of the Storegga Slide, offshore Norway. *Mar. Geol.* **2006**, *229* (3−4), 179−186.
(12) Wang, K.; Chang, Y.; Chen, G.; Sun, B.; Xue, A.; Zhang, Y.; et al. Time-dependent mechanical characteristics of natural gas hydrate production test casing under exploitation disturbance. *J. Nat. Gas Sci. Eng.* **2021**, *94*, No. 104144.
(13) Wang, K.; Chang, Y.; Chen, G.; Sun, B.; Sun, H.; Li, H.; Dai, Y. Three-dimensional mechanical behaviors of casing during gas production from marine hydrate reservoirs using depressurization. *Energy* **2022**, *247*, No. 123526.
(14) Miyazaki, K.; Masui, A.; Sakamoto, Y.; Aoki, K.; Tenma, N.; Yamaguchi, T. Triaxial compressive properties of artificial methane-hydrate-bearing sediment. *J. Geophys. Res.: Solid Earth* **2011**, *116* (B6), No. B06102, DOI: 10.1029/2010JB008049.
(15) Xu, Y.; Song, K.; Wei, J.; Geng, X.; Yao, H.; Wang, W. Experimental study on mechanical property of natural gas hydrate. *Low-Carbon Chem. Chem. Eng.* **2023**, *48* (6), 150−154.
(16) Li, Y.; Wang, L.; Xie, Y.; Wu, P.; Liu, T.; Huang, L.; et al. Deformation characteristics of methane hydrate-bearing clayey and sandy sediments during depressurization dissociation. *Energy* **2023**, *275*, No. 127527.
(17) Ye, J.-l.; Qin, X.-w.; Xie, W.-w.; Lu, H.-l.; Ma, B.-j.; Qiu, H.-j.; et al. The second natural gas hydrate production test in the South China Sea. *China Geol.* **2020**, *3* (2), 197−209.
(18) Lyu, X.; Li, Q.; Ge, Y.; Zhu, J.; Zhou, S.; Fu, Q. Fundamental characteristics of gas hydrate-bearing sediments in the Shenhu area, South China Sea. *Front. Energy* **2021**, *15*, 367−373.
(19) Fu, S.; Lu, J. The characteristics and origin of gas hydrate in Shenhu area, South China Sea. *Mar. Geol. Lett.* **2010**, *26* (9), 6−10.
(20) Tao, L.; Xiao-wei, T. Experimental study on effect of coexistence of clay and silt on static and dynamic liquefaction of sand. *Chin. J. Geotech. Eng.* **2019**, *41* (S2), 169−172.
(21) Jianqun, Z.; Lingwei, K.; Fangjie, Z. Effect of fines content on strength of silty sands. *Chin. J. Geotech. Eng.* **2007**, *29* (11), 1647−1652.
(22) Yongjian, C.; Yanlin, Z.; Songsong, W. Effect of clay content on the strength and compressibility of sandy soil. *Sci. Technol. Eng.* **2017**, *17* (23), 281−286.
(23) Lu, H.; Chen, H.; Chen, F.; Zhiliang, L. Mineralogical characteristics of natural gas hydrate borehole sediments in Shenhu area, South China Sea *Geological Research of South China Sea* 2009, 28 39.
(24) Tang, Q.; Chen, Y.; Jia, R.; Guo, W.; Chen, W.; Li, X.; et al. Effect of clay type and content on the mechanical properties of clayey silt hydrate sediments. *J. Pet. Sci. Eng.* **2023**, *220*, No. 111203.
(25) Wang, B.; Huo, P.; Luo, T.; Fan, Z.; Liu, F.; Xiao, B.; et al. Analysis of the physical properties of hydrate sediments recovered from the Pearl River mouth basin in the South China Sea: Preliminary investigation for gas hydrate exploitation. *Energies* **2017**, *10* (4), 531.
(26) Ma, X.; Jiang, D.; Lu, J.; Fang, X.; Yang, P.; Xia, D. Hydrate formation and dissociation characteristics in clayey silt sediment. *J. Nat. Gas Sci. Eng.* **2022**, *100*, No. 104475.
(27) Shen, S.; Li, Y.; Sun, X.; Wang, L.; Song, Y. Stress behavior of hydrate-bearing sands with changing temperature and hydrate saturation. *J. Nat. Gas Sci. Eng.* **2022**, *98*, No. 104389.
(28) Liu, J.; Zhao, Y.; Sang, S.; Zeng, Z.; Hua, L.; Kong, L. Triaxial tests of hydrate-bearing clayey-silty sediments under different hydrate saturations and effective confining pressures. *Energy Fuels* **2022**, *36* (23), 14042−14054.
(29) Liu, W.; Chen, P.; Wu, P.; You, Z.; Wang, L.; Huang, L.; et al. Mechanical characteristics of underconsolidated methane hydrate-bearing clayed-silty sediments. *Energy Fuels* **2023**, *37* (9), 6503−6514.
(30) Miyazaki, K.; Tenma, N.; Aoki, K.; Yamaguchi, T. A nonlinear elastic model for triaxial compressive properties of artificial methane-hydrate-bearing sediment samples. *Energies* **2012**, *5* (10), 4057−4075.
(31) Song, Y.; Zhu, Y.; Liu, W.; Li, Y.; Lu, Y.; Shen, Z. The effects of methane hydrate dissociation at different temperatures on the stability of porous sediments. *J. Pet. Sci. Eng.* **2016**, *147*, 77−86.
(32) Yu, F.; Song, Y.; Liu, W.; Li, Y.; Lam, W. Analyses of stress strain behavior and constitutive model of artificial methane hydrate. *J. Pet. Sci. Eng.* **2011**, *77* (2), 183−188.
(33) Hyodo, M.; Li, Y.; Yoneda, J.; Nakata, Y.; Yoshimoto, N.; Nishimura, A.; Song, Y. Mechanical behavior of gas-saturated methane hydrate-bearing sediments. *J. Geophys. Res.: Solid Earth* **2013**, *118* (10), 5185−5194.
(34) Yan, R.; Wei, C. Constitutive model for gas hydrate−bearing soils considering hydrate occurrence habits. *Int. J. Geomech.* **2017**, *17* (8), No. 04017032.
(35) Li, Y.H. *Study on strength and deformation behaviors of methane hydrate-bearing sediments [[D]]*. Dalian Univ Technol: 2014.
(36) Zhang, W.; Ma, Q.; Wang, R.; Ren, S. An experimental study of shear strength of gas-hydrate-bearing core samples. *Pet. Sci.* **2011**, *8*, 177−182.
(37) Miyazaki, K.; Masui, A.; Sakamoto, Y.; Tenma, N.; Yamaguchi, T., Eds.; *Effect of Confining Pressure on Triaxial Compressive Properties of Artificial Methane Hydrate Bearing Sediments*, Offshore Technology Conference; OTC, 2010.
(38) Luo, T.; Song, Y.; Zhu, Y.; Liu, W.; Liu, Y.; Li, Y.; Wu, Z. Triaxial experiments on the mechanical properties of hydrate-bearing marine sediments of South China Sea. *Mar. Pet. Geol.* **2016**, *77*, 507−514.
(39) Chen, H.; Du, H.; Shi, B.; Shan, W.; Hou, J. Mechanical properties and strength criterion of clayey sand reservoirs during natural gas hydrate extraction. *Energy* **2022**, *242*, No. 122526.
(40) Zhao, Y.; Kong, L.; Xu, R.; Liu, J.; Sang, S. Strength behaviors of hydrate-bearing clayey-silty sediments with multiple factors. *J. Pet. Sci. Eng.* **2022**, *219*, No. 111035.
(41) Guo, W.; Li, Y.; Jia, R.; Wang, Y.; Tang, G.; Li, X. Experimental study on mechanical properties of pore-filling and fracture-filling clayey silt hydrate-bearing sediments. *Energy* **2023**, *284*, No. 129354.
(42) Zhao, Y.; Kong, L.; Xu, R.; Liu, J.; Sang, S. Mechanical properties of remolded hydrate-bearing clayey-silty sediments. *J. Nat. Gas Sci. Eng.* **2022**, *100*, No. 104473.
(43) Farrokhpay, S.; Ndlovu, B.; Bradshaw, D. Behaviour of swelling clays versus non-swelling clays in flotation. *Miner. Eng.* **2016**, *96-97*, 59−66.
(44) Wang, J.; Wang, S.; Hong, M.; et al. Correlatin Analysis between Clay Mineral Composition and Shear Strength. *J. Southwest Jiaotong Univ.* **2018**, *53* (05), 1033−1038.

https://doi.org/10.1021/acsomega.4c06735
ACS Omega 2024, 9, 46192−46203

(45) Boek, E. S.; Coveney, P.; Skipper, N. Monte Carlo molecular modeling studies of hydrated Li-, Na-, and K-smectites: Understanding the role of potassium as a clay swelling inhibitor. *J. Am. Chem. Soc.* **1995**, *117* (50), 12608−12617.

https://doi.org/10.1021/acsomega.4c06735
ACS Omega 2024, 9, 46192−46203